

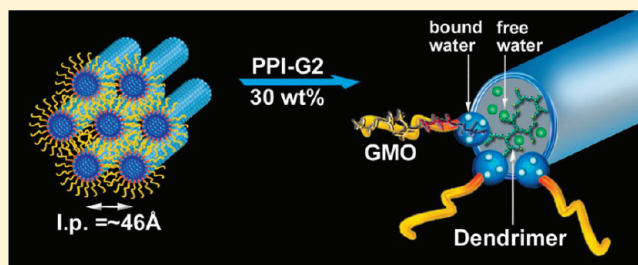
Complex Dendrimer–Lyotropic Liquid Crystalline Systems: Structural Behavior and Interactions

Liron Bitan-Cherbakovsky,[†] Dima Libster,^{*} Abraham Aserin, and Nissim Garti^{*}

The Ratner Chair of Chemistry, Casali Institute of Applied Chemistry, The Institute of Chemistry, The Hebrew University of Jerusalem, Edmond J. Safra Campus, Givat Ram, Jerusalem 91904, Israel

 Supporting Information

ABSTRACT: The incorporation of dendrimer into three lyotropic liquid crystalline (LLCs) mesophases is demonstrated for the first time. A second generation (G2) of poly(propylene imine) dendrimer (PPI) was solubilized into lamellar, diamond reverse cubic, and reverse hexagonal LLCs composed of glycerol monooleate (GMO), and water (and d- α -tocopherol in the H_{II} system). The combination of PPI with LLCs may provide an advantageous drug delivery system. Cross-polarized light microscope, small-angle X-ray scattering (SAXS), and attenuated total reflectance Fourier transform infrared (ATR-FTIR) were utilized to study the structural behavior of the mesophases, the localization of PPI within the system, and the interactions between the guest molecule and the system's components. It was revealed that PPI-G2 functioned as a "water pump", competing with the lipid headgroups for water binding. As a result, L_a→H_{II} and Q²²⁴→H_{II} structural shifts were detected (at 10 wt % PPI-G2 content), probably caused by the dehydration of monoolein headgroups and subsequent increase of the lipid's critical packing parameter (CPP). In the case of H_{II}, as a result of the balance between the dehydration of the monoolein headgroups and the significant presence of PPI within the interfacial region, increasing the quantity of hydrogen bonds, no structural transitions occurred. ATR-FTIR analysis demonstrated a downward shift of the H—O—H (water), as a result of PPI-G2 embedment, suggesting an increase in the mean water—water H-bond angle resulting from binding PPI-G2 to the water network. Additionally, the GMO hydroxyl groups at β - and γ -C—OH positions revealed a partial interaction of hydrogen bonds with N—H functional groups of the protonated PPI-G2. Other GMO interfacial functional groups were shown to interact with the PPI-G2, in parallel with the GMO dehydration phenomenon. In the future, these outcomes can be used to design advanced drug delivery systems, allowing administration of dendrimers as a therapeutic agent from LLCs.



INTRODUCTION

Recently, substantial efforts have been made toward the use of dendrimers as potential drug vehicles or scaffolds.^{1–3} The dendrimers have gained interest in various applications in pharmaceuticals and biomedical systems, especially in the treatment of cancer.⁴ These macromolecules have a unique well-defined "treelike" branching structure, which spreads out from a central core under systematic introduction of branching sites.^{5–7} The beneficial properties of the dendrimers are their low polydispersity and nanosized scale that allow high penetration through the cell membrane and the ability to mimic biomolecules.^{1,4,8} The presence of terminal groups on the dendrimer's surface offers an excellent platform for the attachment of targeting groups, solubility modifiers, and stealth moieties, which reduce immunological interaction.⁹ The three-dimensional structure of dendrimers, consisting of an interior core, interior layer, and exterior surface, possesses the ability to encapsulate bioactive molecules in several sites. These sites include the central core and the flexible space created by the voids in the several interior layers. The drugs may be chemically attached or physically absorbed on

the dendrimers' surface.^{9,10} Alternatively, dendrimers by themselves can serve as therapeutic agents by virtue of their activities against Prion and Alzheimer's disease,¹¹ HIV,¹² cancer, and other diseases.¹³ Dendrimers were shown to prevent formation of amyloid fibrils,¹⁴ destabilize amyloid aggregates,¹⁵ and prevent viral adhesion and replication.¹²

Even though the major advantage of dendrimers is the ability to cross the biological barriers with encapsulated drugs by host–guest interaction, these macromolecules suffer from relatively low encapsulation capacity of various drugs, compared to colloidal carriers. Moreover, it seems that the dendrimers' potential capability to sustain delivery of the encapsulated drugs is much lower compared to that of colloidal vehicles. To improve the performance of dendrimers as delivery agents, we propose a new generation of drug delivery vehicles based on integration of dendrimers and lyotropic liquid crystals. The formation of the

Received: April 3, 2011

Revised: September 4, 2011

Published: September 08, 2011

new complex of dendrimer–lyotropic liquid crystalline (LLC), presented in this paper, may potentially enhance the delivery of dendrimers as a therapeutic agent as a carrier for oral and transdermal release.

Lyotropic liquid crystals are formed by polar lipids and certain surfactant mixing with water.^{16–20} LLCs based on monoglycerides are self-assembled into a large variety of morphologies that exist between isotropic liquid and solid crystalline. Various mesophases can be formed, while the most significant are the lamellar, cubic, and hexagonal structures. The mesophases can be type I (oil-in-water, O/W) or type II (water-in-oil, W/O). These types of LLCs have been shown to provide sustained release of guest molecules with a range of physicochemical properties,²¹ thermodynamic stability, and improved solubility of drugs and bioactive molecules.^{18,22–27}

In the present work, we demonstrate for the first time a complex prospective drug delivery system, based on a dendrimer solubilized in the aqueous domains of lamellar (L_α), reverse bicontinuous diamond cubic, and reverse hexagonal (H_{II}) LLC based on monoglycerides. We utilized LLCs composed of glycerol monooleate (GMO), water,^{17,27,28} and D- α -tocopherol (vitamin E, VE)^{19,26,27} (to form an H_{II} mesophase) and second generation (G2) poly(propylene imine) (PPI) dendrimers. GMO is a polar lipid that is commonly used as a food emulsifier. It is also widely used as a surfactant in systems that encapsulate drug and bioactive molecules.^{22–27} Monoolein is already known for its ability to form several reverse mesophases upon mixing with water, including the lamellar (L_α), bicontinuous cubic (V_I, V_{II}), and reverse hexagonal (H_{II}).^{18,29–31} PPI polycationic dendrimers are of particular interest since they are biocompatible, nontoxic in lower generation,^{32–35} and commercially available.^{2,36} A significant advantage of these polycationic dendrimers is their ability to react with bacterial membranes.³⁷ A second-generation PPI dendrimer possesses eight primary amine groups on the surface.⁶ In aqueous solution at pH < 9.85, most of the PPI-G2 terminal amine groups are protonated and have positive surface charges.^{38,39}

The aim of this work is to explore a model drug delivery system composed of a positively charged PPI-G2 dendrimer entrapped in L_α , Q^D , and H_{II} GMO-based LLCs. To elucidate the effect of the PPI-G2 dendrimer on the three mesophases as a host–guest interaction, we used cross-polarized light microscopy and small-angle X-ray scattering to explore the macrostructural changes and ATR-FTIR to reveal the molecular level interactions.

■ EXPERIMENTAL SECTION

Monoolein, GMO, distilled glycerol monooleate that consists of 97.1 wt % monoglycerides, 2.5 wt % diglycerides, and 0.4 wt % free glycerol (acid value 1.2, iodine value 68.0, melting point 37.5 °C), was purchased from Riken (Tokyo, Japan). D- α -Tocopherol, vitamin E 5–96 (containing 1430 international units of vitamin E), was obtained from ADM (Decatur, IL, USA). PPI (second generation) (>95% purity) was obtained from SyMO-Chem, The Netherlands. Hydrochloric acid 37% was purchased from Sigma-Aldrich (St. Louis, MO, USA). Water was double distilled. All ingredients were used without further purification.

Sample Preparation. The GMO-based LLC samples were formed by adding the dendrimer aqueous phase (solution of PPI-G2 in distilled water at pH = ~8.6–8.7, which formed by HCl

titration to a GMO). At pH = ~8.6–8.7 the PPI dendrimer bears positive charges. Adding 15 and 35 wt % of water–PPI-G2 solution to 85 and 65 wt % of GMO formed the L_α and the Q^D mesophases, respectively. To form the H_{II} mesophase, 20 wt % of water–PPI-G2 solution was added to GMO and VE in a 90/10 wt % ratio. The aqueous phase concentration in each mesophase was kept constant (15, 35, and 20 wt % for L_α , Q^D , and H_{II} , respectively), while the PPI-G2 content in the aqueous phase was 0–30 wt %. After adding the aqueous phase to GMO and to the GMO/VE mixture, the sample was heated to ~70 °C in sealed tubes under nitrogen (to avoid oxidation of the GMO) for ca. 15 min. The samples were stirred and cooled to 25 °C. It should be noted that as a result of PPI-G2 solubilization the concentrations of the water were decreased, keeping the weight ratio of GMO/VE (9:1) and GMO with aqueous phase constant.

Light Microscopy. The samples were inserted between two glass microscope slides and observed with a Nikon light microscope Eclipse 80i model equipped with cross-polarizers and attached to a digital Nikon DXM 1200C camera and PC monitor. The samples were analyzed at room temperature.

Small-Angle X-ray Scattering (SAXS). SAXS measurements were used to identify the structure of the LLC containing various quantities of dendrimer (0–30 wt % in the aqueous phase). The scattering experiments were performed using Ni-filtered Cu K α radiation (0.154) from a Seifert ID 3000 generator that operated at 40 kV, 40 mA at the Nanotechnology Institute, Ben-Gurion University of the Negev, Beer-Sheva, Israel. The spectra were shone through an evacuated compact Kratky camera (Anton PAAR). A linear position-sensitive detector (MBRAUN) was used to record the scattering patterns. The sample-to-detector distance was 280 mm and was calibrated using silver behenate. The samples were held in 1.5 mm quartz X-ray capillaries and were sealed with epoxy. The temperature was maintained at 25 ± 1 °C with an exposure time of ca. 20–60 min. The temperature of the sample holder was controlled by a K-HR (Anton PAAR) temperature controller, and a temperature profile was set by the Anton software. A direct method of the beam-height correction was used for desmearing.⁴⁰ In all scattering patterns, the abscissa is q ($q = 2\pi/d$, where d is the interplanar distance), and the ordinate is the intensity. Scattering curves are normalized with respect to the attenuated main beam.

Attenuated Total Reflectance Fourier Transform Infrared (ATR-FTIR). An Alpha P model spectrophotometer, equipped with a single reflection diamond ATR sampling module, manufactured by Bruker Optik GmbH (Ettlingen, Germany), was used to record the FTIR spectra (GMO/VE/water with AA in different concentrations). The spectra were recorded with 50 scans, with spectral resolution of 2 cm⁻¹, at room temperature. The absorbance intensities reported here were reproducible to ±0.005.

ATR-FTIR Data Analysis. Multi-Gaussian fitting has been utilized to resolve individual bands in the spectra. The peaks were analyzed in terms of peak frequencies, widths at half-height, and areas.

■ RESULTS AND DISCUSSION

Up to 30 wt % PPI-G2 was solubilized into three types of lyotropic liquid crystals (LLC): the lamellar (L_α), the bicontinuous cubic (Q^{224} , $Pn3m$), and the reverse hexagonal (H_{II}) mesophases. The phase behavior as a function of PPI-G2 concentration is covered in the following sections.

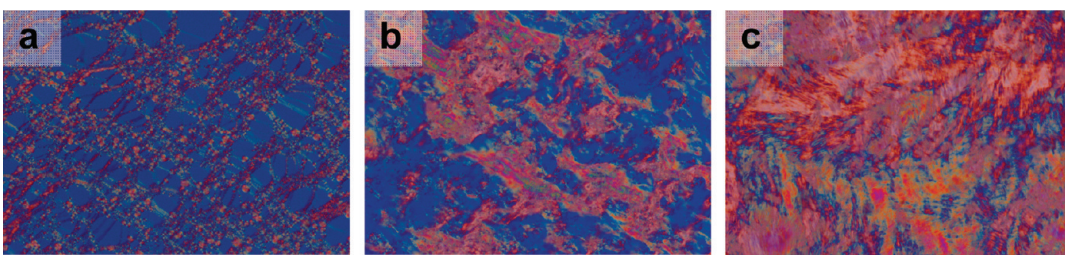


Figure 1. Polarized optical microscope images of L_α and H_{II} liquid crystal systems composed of GMO (85 wt %) and water (15 wt %) containing different concentrations of PPI-G2 from the aqueous phase: 0, 10, and 20 wt % (a, b, and c, respectively). All images were recorded at room temperature with 10 times magnification.

Effect of PPI-G2 on the Lamellar Phase. Macroscopic Characterization by CPLM and SAXS Measurements. The lamellar phase was formed when 15 wt % water was added to the molten GMO.^{18,20} A typical lamellar texture (L_α -phase) was identified by the cross-polarized light microscope as shown in Figure 1a. While at the concentration of PPI-G2 ranging from 0 to 5 wt % the mesophase still retained lamellar symmetry, a two-phase region (L_α and H_{II}) was detected in the presence of 10–20 wt % PPI-G2. Both typical lamellar and hexagonal textures attributed to the L_α and H_{II} symmetries are shown in Figure 1b. The $L_\alpha \rightarrow H_{II}$ transition was completed at 20 wt % PPI-G2, and only the hexagonal mesophase was observed (Figure 1c).

SAXS measurements were carried out to verify the observed transitions. A lamellar spectrum was clearly observed at 0 and 5 wt % PPI-G2, exhibiting a sharp scattering peak (Figure 2A, a). These reflections characterize the inner adjacent bilayer spacing.^{18,20} It should be mentioned that although at least two peaks are supposed to be shown for the L_α symmetry here only one peak appeared. We made our assignment by judging the combined SAXS measurements with the CPLM images and regarding previously published results.⁴¹ When the L_α and H_{II} mesophase mixture was detected, at 10 wt % PPI-G2, the SAXS spectrum was composed of four peaks, corresponding to the L_α and the H_{II} mesophases (Figure 2A, b). For the H_{II} samples, three Bragg peaks were observed, which were indexed as the [10], [11], and [20] reflections of a 2D H_{II} phase (ratios of 1:(3) $^{1/2}$ 2). A spectrum corresponding to the sample containing 20 wt % PPI-G2 with only three Bragg peaks was assigned to the H_{II} mesophase (Figure 2A, c). It should be noted that all these spectra are in line with the microscope images in Figure 1.

Upon increasing the concentration of PPI-G2, the lattice parameter of the L_α mesophase decreased by ~ 3 Å, while the lattice parameter of the H_{II} mesophase exhibited no significant change (Figures 2B and 3A–C). The decrease in the lattice parameter with increasing concentration of PPI-G2 in the lamellar phase can be explained either by dehydration of the lipid polar headgroups or by an increase in its hydrocarbon chains' mobility.^{42,43} Since the PPI-G2 is a water-soluble dendrimer, it may interact with the water network and compete with the monoolein polar heads for water binding. We may assume that the PPI-G2 decreased the cross polar headgroups area (a_0) of the lipid. This resulted in an increase of the effective critical packing parameter (CPP) value of GMO and a subsequent increase in the curvature of the system.⁴⁴ Such a process may induce formation of the H_{II} mesophase possessing high CPP values (~ 1.7) (Figure 3).⁴⁵ A cartoon of the different modifications of the L_α mixture as a function of PPI-G2 concentration is shown in Figure 3, schematically revealing the described structural modifications.

The detected $L_\alpha \rightarrow H_{II}$ transition was further elaborated by ATR-FTIR measurements.

Molecular Level Characterization by ATR-FTIR. ATR-FTIR was used to elucidate the molecular interactions of PPI-G2 within the L_α and H_{II} structures. The spectrum was analyzed in terms of two regions: the water-rich core and the water–surfactant interface, which showed significant modifications in the ATR-FTIR analysis.

The H–O–H bending band at ~ 1650 cm $^{-1}$ was used to characterize the competitive water interactions with the GMO headgroups and the PPI-G2 (Figure 1, Supporting Information) in the water-rich core.

At the interface, the following vibrational modes were analyzed: the stretching bonds of CO–O (ester at the α position, ~ 1180 cm $^{-1}$), C–OH (β , ~ 1121 cm $^{-1}$), C–OH (γ , ~ 1046 cm $^{-1}$), and C=O (carbonyl at the α position, 1720–1740 cm $^{-1}$).^{43,46–48} The carbonyl band consisted of two components, one originating from “free” (freely rotating) carbonyl (1740 cm $^{-1}$) and the second from intramolecular hydrogen-bonded carbonyl groups (1730 cm $^{-1}$).^{47,48}

Water-Rich Core. The reorganization of water upon addition of PPI-G2 was detected by the downward shift of the water bending vibration frequency. This frequency was augmented from 1651 cm $^{-1}$ in the absence of PPI-G2, through ~ 1649 with 15 wt % PPI-G2, and more moderately to 1646 cm $^{-1}$ with 30 wt % PPI-G2 (an overall downward shift of 5 cm $^{-1}$; Figure 1, Supporting Information, first block). It is well documented that the water bending vibration frequency decreases when ionic solutes are introduced to the water as a result of the mean water–water H-bond angle in their first hydration shell.⁴⁹ Ionic solute groups generally increase the root-mean-square (rms) H-bond angle by increasing the population of more distorted H bonds at the expense of the less distorted population.⁴⁹ Since the pH of the PPI-G2 aqueous solution is < 9.85 , most of the PPI-G2 terminal amine groups are protonated and have positive surface charges,^{1,38,39} which make them function as cationic solutes.

Inspecting our results, it could be suggested that a distortion of the water structure upon embedment of the spherical large molecule PPI-G2 took place, increasing the mean water–water H-bond angle.

Upon increasing PPI-G2 content from 0 to 30 wt %, a moderate transition of the γ -C–OH band by 3 cm $^{-1}$ toward lower wavenumbers from 1050 up to 1047 cm $^{-1}$ was obtained (Figure 1, Supporting Information, second block). It is well-known that the downward shift toward lower wavenumber indicates a strong interaction between the polar moieties of the lipid and the water network.⁵⁰ Hence, it was assumed that a partial interaction took place between the PPI-G2–water network and the γ -C–OH groups. This interaction occurred even though

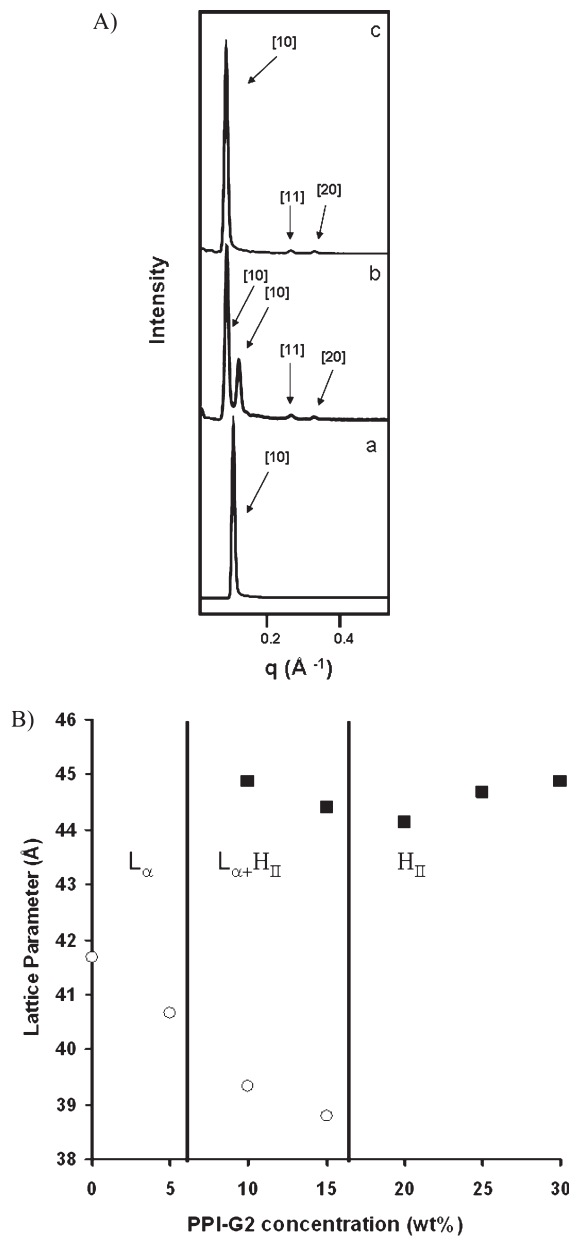


Figure 2. 85 wt % GMO and 15 wt % water + PPI-G2 in variant concentrations (0–30 wt % from the aqueous phase): (A) X-ray diffraction patterns of (a) 0, (b) 10, and (c) 20 wt % PPI-G2 measured at 25 °C. The arrows on traces indicate the locations of the [10], [11], and [20] diffraction peaks. (B) Lattice parameter (\AA) of (○) L_{α} and (■) H_{II} structures as a function of PPI-G2 concentration.

the curvature and the lattice parameter decreased, indicating partial intercalation of PPI-G2 to the lipid–water interfacial region (Figure 3). The β -C–OH stretching vibrations frequency did not reveal a significant change, suggesting no sensitivity to PPI-G2 presence. It can be deduced that hydroxyl groups of the GMO at the γ position were partly hydrogen bonded to the polar groups of the PPI-G2 and water network (i.e., protonated amine).

The changes in the carbonyl bands area and the position upon addition of PPI-G2 are depicted in Figure 1 (Supporting Information, third block). Prior to the incorporation of PPI-G2, the free

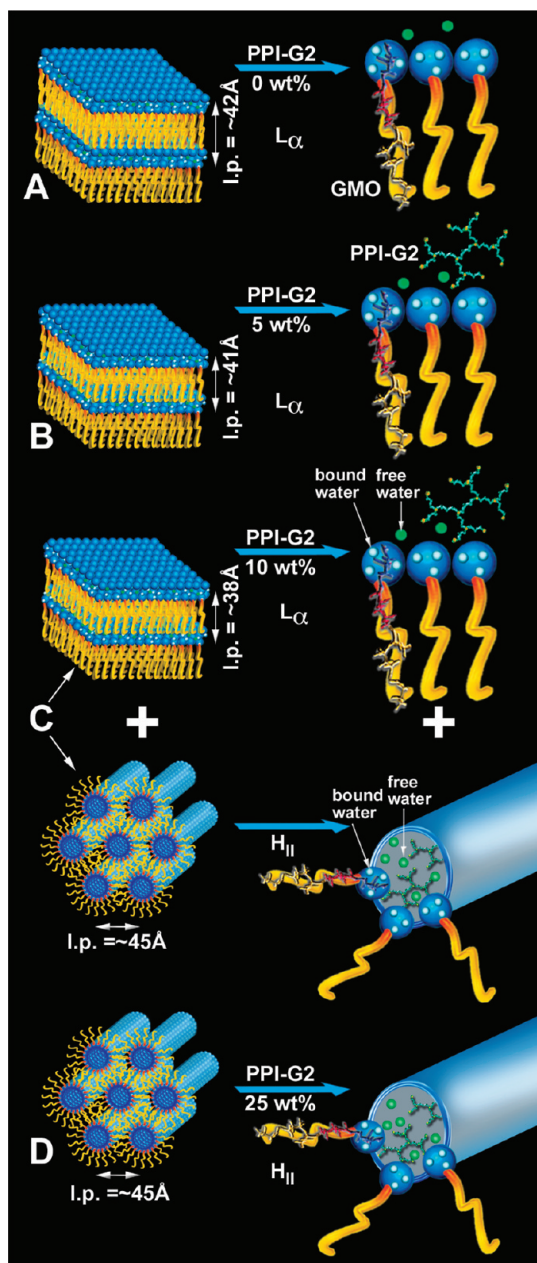


Figure 3. Schematic illustrations of the solubilization location and interactions of protonated PPI-G2 in the L_{α} system. Two major modifications in the L_{α} system are indicated: a reduction in the lattice parameter (i.e., l.p.) and a reduction in the CPP, which caused the $L_{\alpha} \rightarrow H_{\text{II}}$ transition. A and B represent L_{α} mesophases that were formed at 0 and 5 wt % PPI-G2 concentrations in the aqueous phase, respectively. C represents the more significant reduction in lattice parameter and the existence of two phases, L_{α} and H_{II} , when 10 wt % PPI-G2 was solubilized. D represents the existence of the H_{II} mesophase (l.p. = 45 Å) when 25 wt % PPI-G2 was solubilized.

carbonyl band ($\nu_{C=O}$) is detected at 1742 cm^{-1} with an additional higher intensity, bonded carbonyl band at $\sim 1724 \text{ cm}^{-1}$.

The peak areas of both free and bound carbonyls were calculated, and a change in their population was noticed (Figure 2, Supporting Information). In the empty system, the ratio of H-bonded carbonyls to free carbonyls was about 11, while solubilization of 5–10 wt % of the dendrimer molecules into



Figure 4. Polarized optical microscope images of Q^{224} and H_{II} liquid crystal systems composed of GMO (65 wt %) and water (35 wt %) containing different concentrations of PPI-G2 from the aqueous phase: 0, 5, and 20 wt % (a, b, and c, respectively). All images were recorded at room temperature with 10 times magnification.

the mesophase gradually reduced this ratio from 11 to 9. When higher concentrations of PPI-G2 were introduced, an additional drop (from 9 to 6) of the H bonded to free carbonyl occurred. Therefore, the solubilization of the PPI-G2 molecules probably induced partial replacement of the intramolecular H-bonded carbonyl group bonds with carbonyl–PPI-G2 bonds.

It should be mentioned that the frequency of carbonyl groups, free and bound, exhibited no changes upon addition of PPI-G2. Taken together, it was inferred that the partial hydrogen bonds (hydroxyl–carbonyl of GMO) that were disrupted by the PPI-G2 solubilization were reoccupied by N–H groups of PPI-G2 (amine PPI-G2–carbonyl of GMO), mainly at high dendrimer concentrations (greater than 15 wt %).

The $C_\alpha O - O$ stretching mode was detected at $\sim 1171 \text{ cm}^{-1}$. Up to 10 wt % PPI-G2 the frequency decreased to 1170 cm^{-1} , and when more than 15 wt % dendrimer was introduced to the system, it finally reached 1169 cm^{-1} (Figure 1, Supporting Information, fourth block). The transition to low frequency of the $CO - O$ band can be interpreted by a deviation from the dihedral angle of 180° in the $C_\gamma - C_\beta - C_\alpha O - O - C$ segment, induced by torsional motions or by a small population of gauche conformers near the $CO - O$ bond.^{17,41,43,48,51,52} It has been shown that a lower-frequency position of the $CO - O$ band corresponds to more disordered states of the lipids and thus is consistent with the fact that it increases the curvature.^{17,41,43,48,51} This minor decrease of $\sim 2 \text{ cm}^{-1}$ is in line with the SAXS results that showed a drop of the lattice parameter upon the addition of 5–10 wt % PPI-G2 and eventually a transition to H_{II} mesophases at high PPI-G2 concentrations, reflecting an increase in the curvature and a decrease of the a_0 .

Effect of PPI-G2 on the Cubic (Q^{224}) Phase. PPI-G2 was solubilized into the binary Q^{224} bicontinuous diamond cubic phase mesophase^{18,20} composed of GMO (65 wt %) and water (35 wt %). There was no change in the phase symmetry at 5 wt % PPI-G2 concentration (Figure 4 and Figure 5A, a). A reduction of the lattice parameter by $\sim 7.5 \text{ \AA}$ from ~ 125 to $\sim 117.5 \text{ \AA}$ was detected, as examined by SAXS analysis (Figure 6B). When the concentration of PPI-G2 was further increased (10–30 wt %), a $Q^{224} \rightarrow H_{II}$ transition occurred, according to microscopic images and to the SAXS spectrum (Figure 4 and Figures 5A, b and 7a–c).

A significant decrease of up to $\sim 6 \text{ \AA}$ from ~ 52 to $\sim 46 \text{ \AA}$ in the lattice parameter was measured in the presence of 10–30 wt % of the PPI-G2 molecule (Figure 5B). The gradual shrinking of the lattice parameter may point to a partial dehydration of the hydrophilic headgroups of the monoglyceride, probably due to competition for water binding between the PPI-G2 and the polar moieties of the lipid, which caused the $Q^{224} \rightarrow H_{II}$ transition. As the shrinking took place, the curvature of the GMO–water system was increased. As a result, a_0 of the GMO decreased,

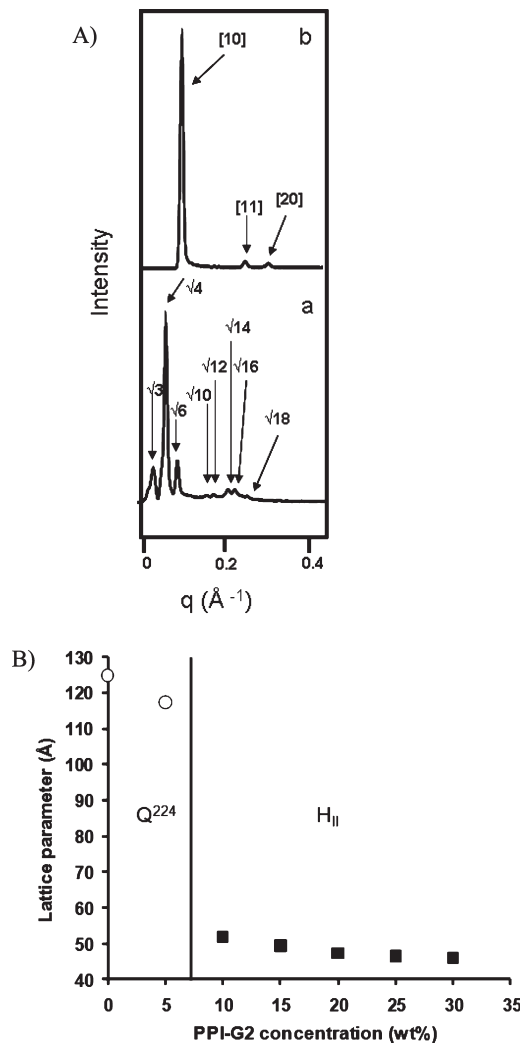


Figure 5. 65 wt % GMO and 35 wt % water + PPI-G2 in variant concentrations (0–30 wt % PPI-G2 from the aqueous phase): (A) X-ray diffraction patterns of (a) 5 and (b) 20 wt % PPI-G2 measured at 25 °C showing the Q^{224} and H_{II} mesophases. (B) Lattice parameter (Å) of (○) Q^{224} and (■) H_{II} .

hence increasing the CPP and inducing the formation of H_{II} mesophases. A detailed illustration representing these structural alterations is shown in Figure 6. It should be noted that the molecular ratio between all the components should not be determined from the image.

To obtain deeper insight into the molecular interactions within the host systems as a result of PPI-G2 solubilization, an

ATR-FTIR analysis was utilized. Examining the O–H bending band, a behavior trend similar to the one observed in the lamellar mesophase was detected. A significant downward shift of $\sim 6 \text{ cm}^{-1}$ (Figure 3, Supporting Information, first block) took place when PPI-G2 was introduced to the mixture at concentrations of 5–30 wt %. This trend is analogous to the effect of PPI-G2 on the lamellar phase, which was explained by the effect of ionic solutes on the water network.

The carbonyl absorption mode was also found to be responsive to PPI-G2 solubilization (Figure 3, second block). Although there were no changes in the position of the bonded and free C=O modes, a trend similar to the lamellar phase in their

population's ratios was observed (Figure 4, Supporting Information). Such conformational modifications, reflected by the changes of normalized areas of C=O low- and high-frequency components, were attributed to a decrease in the average area per headgroup observed upon dehydration of GMO carbonyls as the result of PPI-G2 intercalation.

By analyzing the stretching mode of the C–OH in γ and β positions, we observed a moderate shift toward lower wavenumbers upon increasing the concentration of PPI-G2 (Figure 3, Supporting Information, third block) as we observed in the lamellar phase. As demonstrated in the figure, the significant change was noted at the PPI-G2 concentration range of 5–10 wt %, while only a slight modification was noted when the system had already transformed to the H_{II} mesophase.

A similar phenomenon was noted in the β -C–OH stretching mode as can be seen in Figure 3 (Supporting Information) (overall shift of $\sim 3 \text{ cm}^{-1}$ from 1120 to 1117 cm^{-1} toward lower wavenumbers). Up to 10 wt % PPI-G2, a significant downward transition to lower wavenumbers was recorded from 1120 to 1118 cm^{-1} . In contrast, above 15 wt % of the dendrimer loading, when the mixture completely transformed into hexagonal symmetry, no significant change in the band position was noted. The obtained results led us to assume that at high PPI-G2 concentrations (15–30 wt %) there is a strong binding between N–H groups of the dendrimer and monoolein hydroxyls in the γ and β positions together with C=O–N–H.

Following the interfacial behavior of PPI-G2, the CO–O bond ester stretching mode of the GMO (Figure 3, Supporting Information, fourth block) was examined and exhibited a trend similar to that of the lamellar phase. As already mentioned in the case of the lamellar mesophase, the lower frequency position of the CO–O band that was obtained corresponds to more disordered states of the lipids and thus is consistent with the fact that the curvature of the system was increased as a result of Q²²⁴→H_{II} transition. This outcome is well correlated with the SAXS results that displayed a significant decrease in the lattice parameter at PPI-G2 concentrations above 10 wt %, reflecting an increase in the curvature and finally the structural shift of the Q²²⁴ to H_{II} mesophase.

The described ATR-FTIR results pointed out that the water–lipid interface was notably affected by the PPI-G2 incorporation. Direct interactions of the dendrimer with the GMO hydroxyls, as well as the torsional motion near the CO–O bond, revealed inclusion of the dendrimer into the lipid–water interface. Moreover, PPI-G2 presence in the interface imposed competition for water binding between PPI-G2 and GMO, reflected by the partial dehydration of the GMO carbonyls.

Effect of PPI-G2 on the Reverse Hexagonal (H_{II}) Phase. PPI-G2 was directly incorporated into the hexagonal structures composed of GMO/VE (90:10 ratio)^{19,26,27} and water (20 wt %)

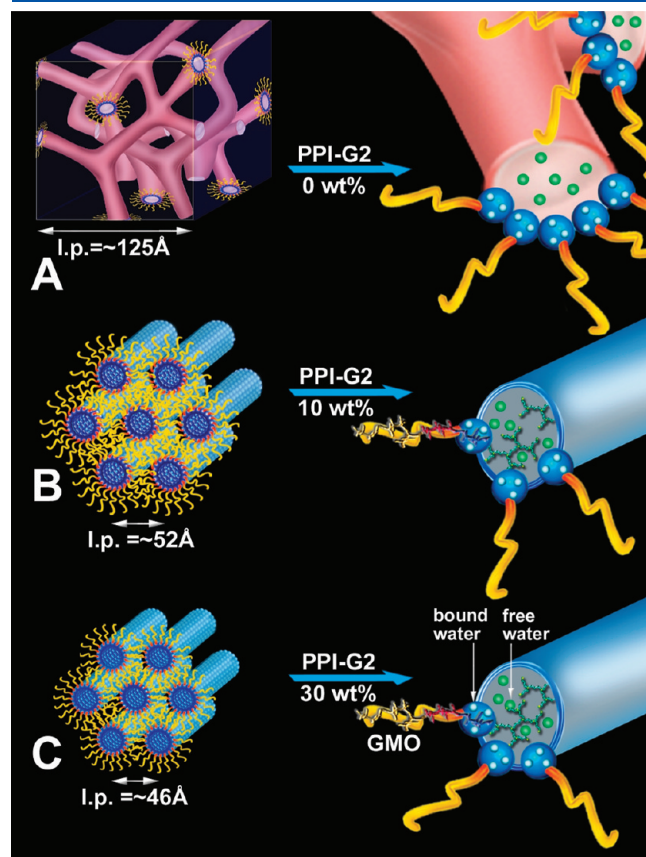


Figure 6. Schematic presentation illustrating the solubilization location and interactions of protonated PPI-G2 in the Q²²⁴ (*Pn3m*) system. Two major modifications are indicated: a reduction in the lattice parameter and a reduction in the CPP, which caused the Q²²⁴→H_{II} transition. (A) The unloaded Q²²⁴ mesophase. (B)+(C) The gradual decrease in lattice parameter and the subsequent formation of the H_{II} mesophase in the presence of 10 and 30 wt % PPI-G2 are shown, respectively.

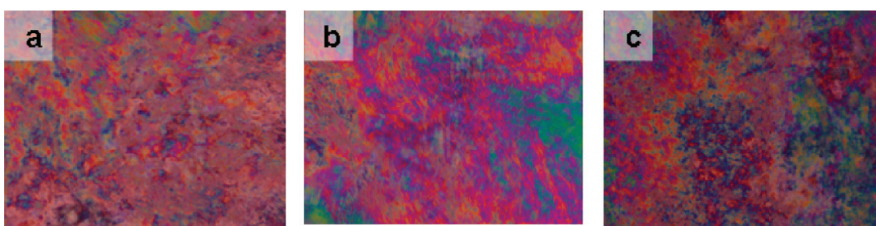


Figure 7. Polarized optical microscope images of H_{II} liquid crystal systems composed of GMO/VE systems (at 90:10 ratio) and water (20 wt %) containing different concentrations of PPI-G2 from the aqueous phase: 0, 5, and 20 wt % (a, b, and c, respectively). All images were recorded at room temperature with 10 times magnification.

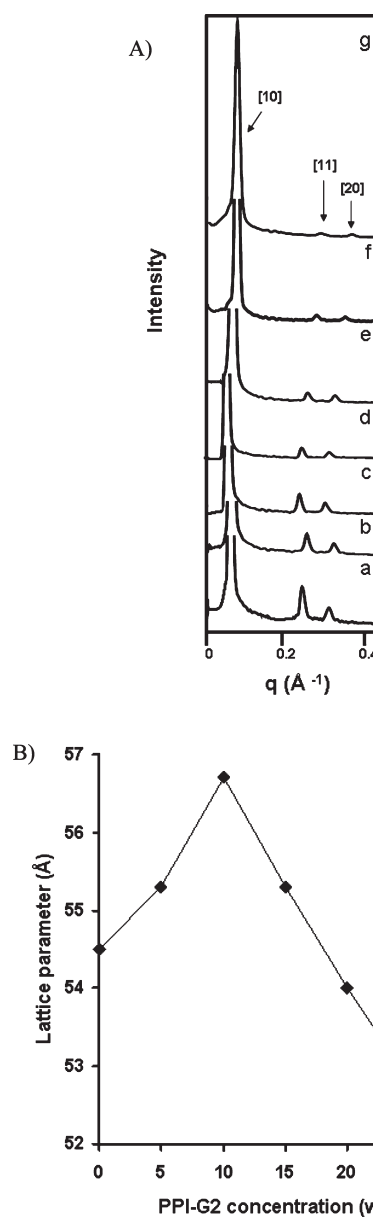


Figure 8. GMO/VE systems (at 90:10 ratio) containing 20 wt % aqueous phase with PPI-G2 in the concentration range of 0–30 wt % from the aqueous phase. (A) X-ray diffraction patterns of: (a) 0 wt %, (b) 5 wt %, (c) 10 wt %, (d) 15 wt %, (e) 20 wt %, (f) 25 wt %, and (g) 30 wt % PPI-G2 measured at 25 °C. The arrows on traces (g) indicate the locations of the [10], [11], and [20] diffraction peaks. (B) Lattice parameter (\AA) of the H_{II} system as a function of PPI-G2 content. The graph represents the two trends that are mentioned in the text.

at a concentration range of 5–30 wt %. According to the microscope observations (Figure 7) and the SAXS measurements (Figure 8A), the hexagonal symmetry was retained over all the examined concentration range.

SAXS measurements demonstrated two trends in the behavior of the lattice parameter (Figure 8B). A minor increase in the lattice parameter values ($\sim 2.5 \text{ \AA}$) from 54.5 \AA to 55.3 \AA was recorded at low concentrations of PPI-G2 (up to 10 wt %). At higher PPI-G2 content (10–30 wt %), the lattice parameter values exhibited a notable decrease of $\sim 4.5 \text{ \AA}$ from 54 to 52.5 \AA (Figures 8B and 9A–C). These results may suggest possible

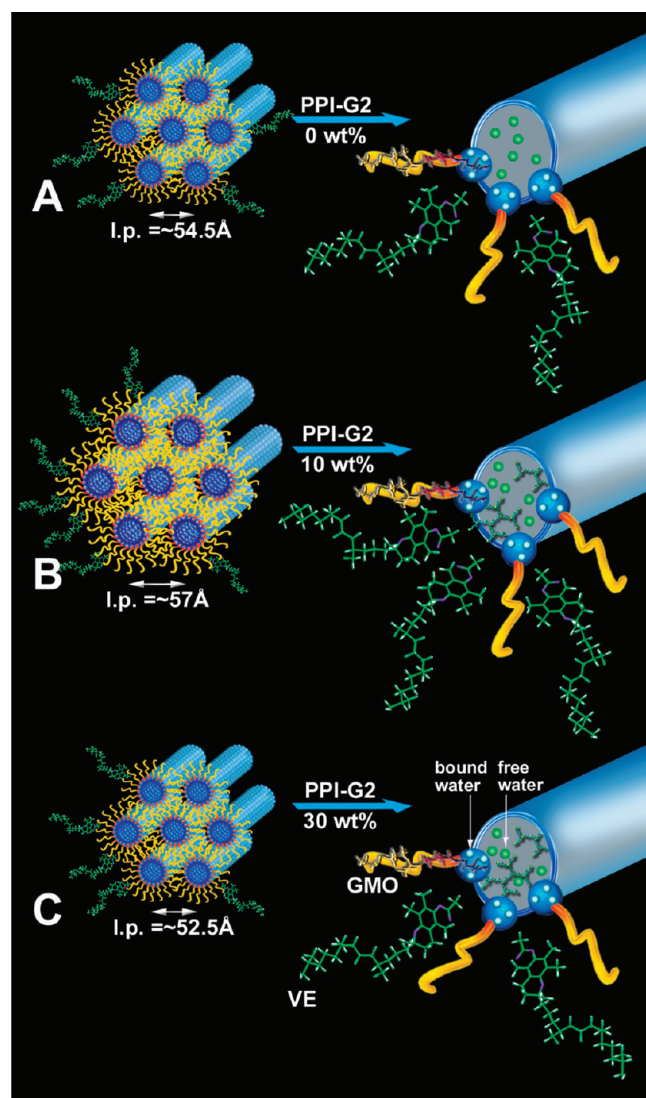


Figure 9. Schematic presentation of the solubilization location and interactions of protonated PPI-G2 in the H_{II} system. Two trends are indicated: an increase of the lattice parameter at 10 wt % PPI-G2 (A, B) and a reduction in the l.p. at 30 wt % of the dendrimer (C).

localization of PPI-G2 within the H_{II} mesophase. In a low concentration region of PPI-G2 (up to 10 wt %), the dendrimer is probably at least partly intercalated into the interface and interacts with the lipid headgroups. This may expand the interface area and thus slightly increase the lattice parameter. However, the interactions of PPI-G2 with water apparently became dominant upon further PPI-G2 solubilization (greater than 10 wt %), leading to dehydration of the GMO headgroups and a reduction in the lattice parameter, similar to the behavior observed in the lamellar and cubic mesophases (Figure 9).

It should be mentioned that the reduction in the lattice parameter did not cause any change in the phase symmetry even though dehydration took place. This special phenomenon can be explained by the delicate balance between the effect of formation of new bonds between PPI-G2 and GMO within the lipid–water interface and the dehydration effect of monoolein headgroups. While the dehydration of GMO polar moieties decreased the

effective headgroups area, a new H-bond formation between PPI-G2 and GMO caused an increase of the headgroups areas. Therefore, the curvature remained in the CPP range, suitable for the existence of the H_{II} structure.

ATR-FTIR analysis enabled us to get deeper insight into the molecular interaction between the components and was well-correlated with the SAXS measurements. Analysis of the peak areas of the free and hydrogen-bonded carbonyl revealed a minor decrease in the bonded $C=O$ population when PPI-G2 was introduced to the mixture (Figure 5, Supporting Information, first block). Taking into consideration the obtained SAXS results, we can assume that the $C=O$ functional groups that were involved in the interactions with O–H groups of the lipid headgroups and water were partially broken and replaced by interactions with N–H functional groups of the dendrimer.

Following the C–OH band in γ and β positions, a downward shift of $\sim 3\text{ cm}^{-1}$ from 1120 to 1117 cm^{-1} was revealed at the β position (Figure 5, Supporting Information, second block). Interestingly, at the γ position no change was observed (Figure 5, Supporting Information, second block). Probably a new H-bond was formed between β -C–OH and N–H groups of the PPI-G2 as a result of the reorganization at the interface. Examining the CO–O stretching mode, similar to the results obtained in the lamellar and cubic mesophases, a more disordered state of lipids was assumed. This outcome is consistent with the decrease of lattice parameter demonstrated by SAXS measurements.

CONCLUSIONS

A composite system based on the integration of the PPI-G2 dendrimer together with LLC was investigated in the current study for the first time. Up to 30 wt % PPI-G2 (from the aqueous phase) was solubilized into the water-rich core and the interfacial region of L_{ω} , Q^{224} , and H_{II} mesophases. Structural transitions, the localization of PPI-G2, and its interaction with the system components were explored by CPLM, SAXS, and ATR-FTIR measurements.

PPI-G2 was found to act as a “water pump” and competed with the lipid headgroups for water binding. This dehydration process probably decreased the area of monoolein polar moieties and induced $L_{\alpha}\rightarrow H_{II}$ and $Q^{224}\rightarrow H_{II}$ structural shifts, as confirmed by microscopic observation and SAXS measurements. As a result of PPI-G2 solubilization in the lamellar mesophase, a reduction in the lattice parameter occurred, accompanied with the formation of the H_{II} mesophase, at PPI-G2 content of 5–15 wt %. The $L_{\alpha}\rightarrow H_{II}$ structural transition was completed upon addition of 25 wt % PPI-G2.

Solubilization of PPI-G2 into the Q^{224} phase caused a phase transition to the H_{II} mesophase starting from 10 wt % PPI-G2. Likewise, in the case of the lamellar phase, this transition was derived from the dehydration of monoolein polar headgroups and subsequent induced increase of the lipid's CPP. At the same PPI-G2 content (10 wt %) within L_{ω} , Q^{224} , and H_{II} mesophases, structural transitions took place only in the lamellar and cubic mesophases, while the hexagonal symmetry was retained. This was explained by a balance between two competing processes. The first was the dehydration of the monoolein headgroups, reducing their area. The second was strong intercalation of the macromolecules to the interfacial region, increasing the number of hydrogen bonds there. This delicate balance probably prevented drastic curvature alterations of the H_{II} mesophase.

ATR-FTIR analysis confirmed the strong binding of PPI-G2 to water and the competition with the lipid headgroups. A considerable shift to lower wavenumbers of the H–O–H functional groups of the water, as a result of the PPI-G2 solubilization, led us to conclude that an increase in the mean water–water H-bond angle took place by binding PPI-G2 to the water network. Examination of the hydroxyl groups of GMO at γ - and β -C–OH positions revealed a partial interaction of hydrogen bonds with N–H functional groups of the protonated PPI-G2. Moreover, the fact that the number of hydrogen-bonded carbonyls did not increase confirmed this interaction. It was probably induced by the replacement of the intramolecular hydrogen-bonded carbonyl group bonds with carbonyl–PPI-G2 bonds. These outcomes reinforced the conclusion that interfacial interactions occurred together with dehydration.

A reduction in the stretching mode frequency of CO–O bands indicated a more disordered state of the lipids, which was consistent with the reduction in the polar headgroups area and observed structural transitions.

A potential drug delivery system, based on dendrimer incorporated into the aqueous domains of LLC, is proposed as an outcome of this work. This system can be further used for entrapment of bioactive guest molecules and study of their delivery profiles as will be shown in our next manuscript.

ASSOCIATED CONTENT

S Supporting Information. Additional Figures 1–5. This material is available free of charge via the Internet at <http://pubs.acs.org>.

AUTHOR INFORMATION

Corresponding Author

*Prof. Nissim Garti. Tel.: +972-2-658-6574/5. Fax: +972-2-652-0262. E-mail: garti@vms.huji.ac.il. Dr. Dima Libster. Tel.: +972-2-658-4962. Fax: +972-2-652-0262. E-mail: dima.libster@mail.huji.ac.il.

Notes

[†]The results presented in this manuscript will appear in the Ph.D. dissertation of L.B.-C. in partial fulfillment of the requirements for the Ph.D. degree in Chemistry, The Hebrew University of Jerusalem, Israel.

ACKNOWLEDGMENT

We would like to thank Dr. S. Vanounou from the Nanotechnology Institute, Ben-Gurion University of the Negev, Beer-Sheva, Israel, for help in measuring the SAXS samples.

REFERENCES

- (1) Nir, I.; Aserin, A.; Libster, D.; Garti, N. *J. Phys. Chem. B* **2010**, *114*, 16723–16730.
- (2) Cheng, Y.; Xu, T. *Eur. J. Med. Chem.* **2008**, *43*, 2291–2297.
- (3) Feng, X.; Cheng, Y.; Yang, K.; Zhang, J.; Wu, Q.; Xu, T. *J. Phys. Chem. B* **2010**, *114*, 11017–11026.
- (4) Wolinsky, J. B.; Grinstaff, M. W. *Adv. Drug Delivery Rev.* **2008**, *60*, 1037–1055.
- (5) Cheng, Y.; Wu, Q.; Li, Y.; Hu, J.; Xu, T. *J. Phys. Chem. B* **2009**, *113*, 8339–8346.

- (6) Scherrenberg, R.; Coussens, B.; van Vliet, P.; Edouard, G.; Brackman, J.; de Brabander, E.; Mortensen, K. *Macromolecules* **1998**, *31*, 456–461.
- (7) Nandy, B.; Maiti, P. K. *J. Phys. Chem. B* **2011**, *115*, 217–230.
- (8) Venditto, V. J.; Regino, C. A. S.; Brechbiel, M. W. *Mol. Pharmaceutics* **2005**, *2*, 302–311.
- (9) Tomalia, D. A.; Reyna, L. A.; Svenson, S. *Biochem. Soc. Trans.* **2007**, *35*, 61–67.
- (10) Jang, W. D.; Selim, K. M. K.; Lee, Ch. H.; Kang, I. K. *Prog. Polym. Sci.* **2009**, *34*, 1–23.
- (11) Klajnert, B.; Cortijo-Arellano, M.; Bryszewska, M.; Cladera, J. *Biochem. Biophys. Res. Commun.* **2006**, *339*, 577–582.
- (12) Witvrouw, M.; Fikkert, V.; Pluymers, W.; Matthews, B.; Mardel, K.; Schols, D.; Raff, J.; Debyser, Z.; De Clercq, E.; Holan, G.; Panneconeque, C. *Mol. Pharmacol.* **2000**, *58*, 1100–1108.
- (13) Gajbhiye, V.; Palanirajan, V. K.; Tekade, R. K.; Jain, N. K. *J. Pharm. Pharmacol.* **2009**, *61*, 989–1003.
- (14) Klajnert, B.; Cortijo-Arellano, M.; Cladera, J.; Bryszewska, M. *Biochem. Biophys. Res. Commun.* **2006**, *345*, 21–28.
- (15) Heegaard, P. M. H.; Pedersen, H. G.; Flink, J.; Boas, U. *FEBS Lett.* **2004**, *577*, 127–133.
- (16) Mezzenga, R.; Meyer, C.; Servais, C.; Romoscanu, A. I.; Sagalowicz, L.; Hayward, R. C. *Langmuir* **2005**, *21*, 3322–3333.
- (17) Libster, D.; Ben Ishai, P.; Aserin, A.; Shoham, G.; Garti, N. *Langmuir* **2008**, *24*, 2118–2127.
- (18) Amar-Yuli, I.; Garti, N. *Colloids Surf. B* **2005**, *43*, 72–82.
- (19) Bitan-Cherbakovsky, L.; Yuli-Amar, I.; Aserin, A.; Garti, N. *Langmuir* **2009**, *25*, 13106–13113.
- (20) Hyde, S. T. In *Handbook of Applied Surface and Colloid Chemistry*; Holmberg, K., Ed.; Wiley: New York, 2001; pp 299–332, Chapter 16.
- (21) Drummond, C. J.; Fong, C. *Curr. Opin. Colloid Interface Sci.* **2000**, *4*, 449–456.
- (22) Libster, D.; Aserin, A.; Wachtel, E.; Shoham, G.; Garti, N. *J. Colloid Interface Sci.* **2007**, *308*, 514–524.
- (23) Libster, D.; Aserin, A.; Yariv, D.; Shoham, G.; Garti, N. *J. Phys. Chem. B* **2009**, *113*, 6336–6346.
- (24) Mishraki, T.; Libster, D.; Aserin, A.; Garti, N. *Colloids Surf. B* **2010**, *75*, 47–56.
- (25) Cohen-Avrahami, M.; Aserin, A.; Garti, N. *Colloids Surf. B* **2010**, *77*, 131–138.
- (26) Bitan-Cherbakovsky, L.; Yuli-Amar, I.; Aserin, A.; Garti, N. *Langmuir* **2010**, *26*, 3648–3653.
- (27) Amar-Yuli, I.; Aserin, A.; Garti, N. *J. Phys. Chem. B* **2008**, *112*, 10171–10180.
- (28) Efrat, R.; Kesselman, E.; Aserin, A.; Garti, N.; Danino, D. *Langmuir* **2009**, *25*, 1316–1326.
- (29) Shan-Yang, L.; Hsiu-Li, L.; Mei-Jane, L. *Adsorption* **2002**, *8*, 197–202.
- (30) Jensen, J. W.; Schutzbach, J. S. *Biochemistry* **1984**, *23*, 1115–1119.
- (31) Rilfors, L. *Biochim. Biophys. Acta* **1985**, *813*, 151–160.
- (32) Jain, K.; Kesharwani, P.; Gupta, U.; Jain, N. K. *Int. J. Pharm.* **2010**, *394*, 122–142.
- (33) Hollins, A. J.; Omidi, Y.; Benter, I. F. *J. Drug Target* **2007**, *15*, 83–88.
- (34) Akhtar, S.; Benter, I. *Adv. Drug Delivery Rev.* **2007**, *59*, 164–182.
- (35) Zinselmeyer, B. H.; Mackay, S. P.; Schatzlein, A. G.; Uchegbu, L. F. *Pharm. Res.* **2002**, *19*, 960–967.
- (36) Nanjwade, B. K.; Bechra, H. M.; Derkar, G. K.; Manvi, F. V.; Nanjwade, V. K. *Eur. J. Pharm. Sci.* **2009**, *38*, 185–196.
- (37) Chen, C. Z. S.; Cooper, S. L. *Biomaterials* **2002**, *23*, 3359–3368.
- (38) Kabanov, V. A.; Zezin, A. B.; Rogacheva, V. B.; Gulyaeva, Z. G.; Zansochova, M. F.; Joosten, J. G. H.; Brackman, J. *Macromolecules* **1998**, *31*, 5142–5144.
- (39) van Duijvenbode, R. C.; Borkovec, M.; Koper, G. J. M. *Polymer* **1998**, *39*, 2657–2664.
- (40) Singh, M. A.; Ghosh, S. S.; Shannon, R. F. *J. Appl. Crystallogr.* **1993**, *26*, 787–794.
- (41) Amar-Yuli, I.; Wachtel, E.; Shalev, D.; Moshe, H.; Aserin, A.; Garti, N. *J. Phys. Chem. B* **2007**, *111*, 13544–13553.
- (42) Caffrey, M. *Biochemistry* **1987**, *26*, 6349–6363.
- (43) Amar-Yuli, I.; Wachtel, E.; Ben-Shoshan, E.; Danino, D.; Aserin, A.; Garti, N. *Langmuir* **2007**, *23*, 3637–3645.
- (44) Sagnella, S. M.; Conn, C. E.; Krodkiewska, I.; Moghaddam, M.; Drummond, C. J. *J. Phys. Chem. B* **2010**, *114*, 1729–1737.
- (45) Borné, J.; Nylander, T.; Khan, A. *Langmuir* **2000**, *16*, 10044–10054.
- (46) Nilsson, A.; Holmgren, A.; Lindblom, G. *Biochemistry* **1991**, *30*, 2126–2133.
- (47) Nilsson, A.; Holmgren, A.; Lindblom, G. *Chem. Phys. Lipids* **1994**, *71*, 119–131.
- (48) Razumas, V.; Larsson, K.; Miezis, Y.; Nylander, T. *J. Phys. Chem.* **1996**, *100*, 11766–11774.
- (49) Sharp, K. A.; Madan, B.; Manas, E.; Vanderkooi, J. M. *J. Chem. Phys.* **2001**, *114*, 1791–1796.
- (50) Severcan, F. *Biosci. Rep.* **1997**, *17*, 231–235.
- (51) Hubner, W.; Mantsch, H. H. *Biophys. J.* **1991**, *59*, 1261–1272.
- (52) Achrai, B.; Libster, D.; Aserin, A.; Garti, N. *J. Phys. Chem. B* **2011**, *115*, 825–835.